Journal of Power Sources 206 (2012) 171–178

Contents lists available at SciVerse ScienceDirect

Journal of Power Sources

journal homepage: www.elsevier.com/locate/jpowsour

A modified dusty gas model in the form of a Fick's model for the prediction of multicomponent mass transport in a solid oxide fuel cell anode

Wei Kong[a], Huayang Zhu[b], Zaiyao Fei[a], Zijing Lin[a,*]

[a] Department of Physics and National Synchrotron Radiation Laboratory, University of Science and Technology of China, Hefei 230026, China
[b] Engineering Division, Colorado School of Mines, Golden, CO 80401, USA

ARTICLE INFO

Article history:
Received 15 December 2011
Accepted 1 January 2012
Available online 25 January 2012

Keywords:
Mass transport
Porous media
Dusty gas model
Fick's model
Solid oxide fuel cell

ABSTRACT

The dusty gas model (DGM) is accurate but difficult to use for describing multicomponent mass transport in porous media. Based on a reasonable approximation that is exact for binary mixtures, the DGM is reformulated in the form of a Fick's model with explicit analytical expressions for the flux of each species. The validity of the new formulation, the DGMFM, is tested using a numerical model of a solid oxide fuel cell (SOFC) anode with realistic microstructure data and partially reformed methane fuel. Methane steam reforming and the water gas-shift reaction in the anode are included in the model. The accuracy of the DGMFM is checked by systematically varying the factors that may affect the mass transport in the porous anode, such as the pore radius, porosity, tortuosity factor, anode thickness, temperature, current density and fuel composition. The comprehensive study shows conclusively that the DGMFM is highly accurate in reproducing the DGM results for all practical SOFC operations.

1. Introduction

Solid oxide fuel cells (SOFCs) have received increasing attention in recent years due to their high efficiency and fuel flexibility in comparison with low-temperature fuel cells [1–3]. Hydrogen, carbon monoxide, natural gas, and other hydrocarbons may be used as fuels with internal steam reforming due to their high operating temperature [2]. SOFCs working at intermediate temperatures (650–800 °C) are seen as the best compromise for reducing the effect of the operating temperature on the SOFC materials while maintaining the benefit of fuel flexibility [4]. Anode-supported SOFCs are suited for operation at intermediate temperatures due to their use of a very thin electrolyte layer that drastically reduces the electrolyte ohmic polarization [5,6]. However, the concentration polarization on the anode side makes a significant contribution to the voltage losses in an anode-supported SOFC, especially at a high fuel utilization or a high operating current density [7,8], as the relatively thick anode hinders the supply of reactant gases to the reaction sites and the elimination of the product gases from the reaction sites. A comprehensive mass-transfer model that is capable of accurately describing the fuel gas transport in a porous anode is very important for the understanding and prediction of fuel cell performance and for the design optimization of porous anode structures.

Mass transport in porous media is complex and generally includes three distinct mechanisms: Knudsen diffusion, molecular diffusion and viscous flow [9,10]. The relative importance of the three mechanisms can be determined from the Knudsen number (*Kn*), a dimensionless number that is defined as the ratio of the molecular mean free path length to a representative physical length scale (the pore diameter in the case of porous media) [9,11]. When *Kn* is much larger than 10, the collision of the gas molecules with the solid walls of porous materials is more important than the collisions between the gas molecules. As a result, viscous flow and molecular diffusion are negligible in comparison with Knudsen diffusion. When *Kn* is much smaller than 0.1, collisions between the gas molecules and the solid wall are rare, and viscous flow and molecular diffusion dominate the overall mass-transfer process. For *Kn* in the intermediate range of 0.1–10, however, collisions among molecules and with pore walls are similarly important, and all three mass transfer mechanisms should be accounted for in this transition regime. In an SOFC, the pore size typically lies in the range 0.05–1 μm [8,12–15], whereas the mean free path for typical gas molecules under working conditions is on the order of 0.2 μm. Therefore, mass transport inside the porous SOFC electrodes falls in the diffusion transition regime.

There are four theoretical models for mass transport in porous media that are widely used in the literature. Fick's model (FM) is the simplest approach to gas diffusion [10,16]. FM postulates that the flux always moves from regions of higher concentration to regions of lower concentration and that the flux is proportional to the concentration gradient of that species. The advective-diffusive model

* Corresponding author. Tel.: +86 551 3606345; fax: +86 551 3606348.
E-mail address: zjlin@ustc.edu.cn (Z. Lin).

0378-7753/$ – see front matter © 2012 Elsevier B.V. All rights reserved.
doi:10.1016/j.jpowsour.2012.01.107

(ADM) [17] is an extended FM that linearly combines the molecular diffusion and viscous flow with the molecular diffusion calculated by FM and the viscous flow predicted by Darcy's law. Because FM and the ADM only account for one-way interactions between the solvent and the solutes [10], they are valid only for binary mixtures or dilute solutions without electrostatic or centrifugal force fields [10,18,19]. For multicomponent diffusion and concentrated mixtures, FM and the ADM have serious limitations [10,20–22], and the Stefan–Maxwell model (SMM) is recommended [10,22,23], which was developed on the basis of kinetic theory and takes into account the interactions among the molecules. The SMM has been used successfully in many fields, including diffusion in distillation, diffusion in an electrostatic force field and diffusion in a centrifugal force field [10]. However, the SMM does not consider the collision of the gas molecules with the pore walls and cannot accurately describe gas diffusion in porous media [17]. The DGM [10,24] addresses many of the shortcomings of FM, the ADM or the SMM for gas transport in the diffusion transition regime. The predictive capability of the DGM is well documented [10,24], and the DGM is the method of choice for gas transport in porous media.

Although the superiority of the DGM is well established and the deficiency of FM and the ADM is well known (as in much of the literature, for convenience, FM refers to both FM and the ADM in the rest of the paper), FM is still the most commonly used method for the prediction of fluxes inside porous media [17,25–27]. This unfortunate situation may be mainly attributed to the following reasons: first, FM gives an explicit analytical expression for the flux of each species that may be used directly in the mass conservation equation to obtain the concentration distribution of the species. However, the fluxes of different species are coupled with one another in the DGM, and further coupling of the DGM with the mass conservation equations and the bulk chemical reactions is cumbersome to perform. Second, the nonlinear coupled partial differential equations of the DGM are often difficult to solve. This is particularly the case when a large number of species is involved. Third, a theoretical analysis of SOFCs often must rely on commercial software such as FLUENT [28], CFX [29] or COMSOL [30] that requires uncoupled expressions for the fluxes of the species. FM is well suited to commercial software, but the DGM is often a challenge for commercial software. Therefore, it is highly desirable to recast the DGM in the form of an FM. The DGM in the form of an FM (DGMFM) would enable the widespread application of the accurate analysis of mass transport in porous electrodes by the general SOFC community. The DGMFM would also find applications in many other fields dealing with the mass transport of multicomponent mixtures in porous media, such as membrane distillation [31], porous catalysts [32], subterranean contaminant migration [33,34], gas-cooled nuclear reactors [35], and others.

In this paper, an effective DGMFM is derived from the DGM based on a reasonable approximation that is exact for binary mixtures. The accuracy of this DGMFM for applications to the analysis of an SOFC is tested by systematically varying the working parameters, such as the pore radius, porosity, tortuosity factor, anode thickness, fuel composition, temperature and operating current density.

2. Theory

The DGM in molar units has the form [10,24,36]:

$$\frac{N_i}{D_{iK}^{eff}} + \sum_{j=1}^{n} \frac{x_j N_i - x_i N_j}{D_{ij}^{eff}} = -\frac{1}{RT}\left(p\nabla x_i + x_i \nabla p + x_i \nabla p \frac{kp}{D_{iK}^{eff}\mu}\right) \quad (1)$$

where N_i is the molar flux of species i, $x_i (= c_i/c_{tot})$ is the molar fraction of species i, c_i is the molar concentration of species i, $c_{tot} (= \sum_j c_j)$ is the total molar concentration of the mixture, R is the universal gas constant, T is the absolute temperature, p is the total gas pressure, k is the permeability coefficient, μ is the viscosity coefficient, D_{iK}^{eff} is the effective Knudsen diffusion coefficient of species i and D_{ij}^{eff} is the effective binary diffusion coefficient.

D_{ij}^{eff} and D_{iK}^{eff} may be evaluated by the following equations [16,37,38]:

$$D_{ij}^{eff} = D_{ji}^{eff} = \frac{\varepsilon}{\tau}\frac{3.198\times 10^{-8} T^{1.75}}{p\left(\nu_i^{1/3} + \nu_j^{1/3}\right)^2}\left(\frac{1}{M_i} + \frac{1}{M_j}\right)^{0.5} \quad (2)$$

$$D_{iK}^{eff} = \frac{\varepsilon}{\tau}\frac{2}{3} r_g \sqrt{\frac{8RT}{\pi M_i}} \quad (3)$$

where ε is the porosity, τ is the tortuosity factor, r_g is the pore radius, and ν_i and M_i are the diffusion volume and molar mass, respectively, of species i.

For $i = l$, Eq. (1) becomes:

$$\frac{N_l}{D_{lk}^{eff}} + \sum_{j=1}^{n} \frac{x_j N_l - x_l N_j}{D_{lj}^{eff}} = -\frac{1}{RT}\left(p\nabla x_l + x_l \nabla p + x_l \nabla p \frac{kp}{D_{lk}^{eff}\mu}\right) \quad (4)$$

Rearranging Eq. (4) yields:

$$-\left(\sum_{j\neq l}\frac{N_j}{D_{lj}^{eff}}\right)x_l + \left(\frac{1}{D_{lk}^{eff}} + \sum_{j\neq 1}\frac{x_j}{D_{lj}^{eff}}\right)N_l = -\frac{1}{RT}\left(p\nabla x_l + x_l\nabla p + x_l \nabla p\frac{kp}{D_{lk}^{eff}\mu}\right) \quad (5)$$

Eq. (5) may be rewritten as:

$$-\frac{y_2}{\tilde{D}_{21}^{eff}}\tilde{N}_1 + \left(\frac{1}{\tilde{D}_{2K}^{eff}} + \frac{y_1}{\tilde{D}_{21}^{eff}}\right)\tilde{N}_2 = -\frac{1}{RT}\left(p\nabla y_2 + y_2\nabla p + y_2\nabla p\frac{kp}{\mu}\frac{1}{\tilde{D}_{2K}^{eff}}\right) \quad (6)$$

where $y_2 = x_l$ and $\tilde{D}_{2K}^{eff} = D_{lK}^{eff}$, as is evident by comparing the right-hand sides of Eqs. (5) and (6). Defining $\tilde{N}_2 = N_l$ and $y_1 = 1 - y_2 = \sum_{i\neq l} x_i$ and comparing the left-hand sides of Eqs. (5) and (6) gives:

$$\tilde{D}_{21}^{eff} = \frac{y_1}{\sum_{j\neq l}(x_j/D_{lj}^{eff})} = \frac{1-x_l}{\sum_{j\neq l}(x_j/D_{lj}^{eff})}\bar{Y} \quad (7)$$

$$\tilde{N}_1 = \frac{\tilde{D}_{21}^{eff}}{y_2}\left(\sum_{j\neq l}\frac{N_j}{D_{lj}^{eff}}\right)x_l = \tilde{D}_{21}^{eff}\left(\sum_{j\neq l}\frac{N_j}{D_{lj}^{eff}}\right) \quad (8)$$

Summing Eq. (1) over all i other than l yields:

$$\sum_{i\neq l}\frac{N_i}{D_{ik}^{eff}} + \sum_{i\neq l}\sum_{D_{ij}^{eff}}^{n}\frac{x_j N_i - x_i N_j}{D_{ij}^{eff}} = -\frac{1}{RT}\left(p\sum_{i\neq l}\nabla x_i + \nabla p\sum_{i\neq l}x_i + \nabla p\frac{kp}{\mu}\sum_{i\neq l}\frac{x_i}{D_{ik}^{eff}}\right) \quad (9)$$

The double summations over i and j of the second term on the left-hand side of Eq. (9) cancel each other except for when $j = l$:

$$-\sum_{i\neq l}\frac{N_i}{D_{iK}^{eff}}+\sum_{i\neq l}\frac{x_lN_i-x_iN_l}{D_{il}^{eff}} = -\frac{1}{RT}\left(p\sum_{i\neq l}\nabla x_i+\nabla p\sum_{i\neq l}x_i+\nabla p\frac{kp}{\mu}\sum_{i\neq l}\frac{x_i}{D_{iK}^{eff}}\right). \quad (10)$$

Rearranging Eq. (10) gives:

$$\left(-\sum_{i\neq l}\frac{x_i}{D_{il}^{eff}}\right)N_l+\sum_{i\neq l}\left[\left(\frac{1}{D_{iK}^{eff}}+\frac{x_l}{D_{il}^{eff}}\right)N_i\right] = -\frac{1}{RT}\left(p\sum_{i\neq l}\nabla x_i+\nabla p\sum_{i\neq l}x_i+\nabla p\frac{kp}{\mu}\sum_{i\neq l}\frac{x_i}{D_{iK}^{eff}}\right) \quad (11)$$

Eq. 11 may be written as:

$$-\frac{y_1}{\tilde{D}_{12}^{eff}}\tilde{N}_2+\left(\frac{1}{\tilde{D}_{1K}^{eff}}+\frac{y_2}{\tilde{D}_{12}^{eff}}\right)\tilde{N}_1-\Delta = -\frac{1}{RT}\left(p\nabla y_1+y_1\nabla p+y_1\nabla p\frac{kp}{\mu}\frac{1}{\tilde{D}_{1K}^{eff}}\right) \quad (12)$$

where $\tilde{D}_{1k}^{eff}=y_1/\sum_{i\neq l}(x_i/D_{ik}^{eff})=(1-x)/\sum_{i\neq l}(x_i/D_{ik}^{eff})$, which is deduced by comparing the right-hand sides of Eqs. (11) and (12). Comparing the left-hand sides of Eqs. (11) and (12) yields: $\tilde{D}_{12}^{eff}=y_1/\sum_{i\neq l}(x_i/D_{il}^{eff})=\tilde{D}_{21}^{eff}$ and $\Delta=(\tilde{D}_{21}^{eff}/\tilde{D}_{1K}^{eff})\sum_{i\neq l}(N_i/D_{li}^{eff})-\sum_{i\neq l}(N_i/D_{iK}^{eff})$.

The following equation is obtained from Eq. (12):

$$\tilde{N}_1=\left(\frac{\tilde{D}_{1K}^{eff}\tilde{D}_{12}^{eff}}{\tilde{D}_{12}^{eff}+\tilde{D}_{1K}^{eff}y_2}\right)\times\left(\frac{y_1}{\tilde{D}_{12}^{eff}}\tilde{N}_2+\Delta-\frac{1}{RT}\left(p\nabla y_1+y_1\nabla p+y_1\nabla p\frac{kp}{\mu}\frac{1}{\tilde{D}_{1K}^{eff}}\right)\right) \quad (13)$$

Inserting Eq. (13) into Eq. (6) gives:

$$N_l=\overline{N}_2=-\overline{D_2}\nabla\overline{c_2}-\overline{c_2}\frac{\overline{k_2}}{\mu}\nabla p+\overline{N_2^{\delta}}=N_l^{diffusion}+N_l^{convection}+N_l^{\delta} \quad (14)$$

where

$$\overline{c_2}=y_2c_t=c_l \quad (15a)$$

$$\overline{D_2}=\left(\frac{\tilde{D}_{12}^{eff}\tilde{D}_{2K}^{eff}}{\tilde{D}_{12}^{eff}+y_2\tilde{D}_{1K}^{eff}+y_1\tilde{D}_{2K}^{eff}}\right) \quad (15b)$$

$$N_l^{diffusion}=-\overline{D_2}\nabla\overline{c_2} \quad (15c)$$

$$\overline{k_2}=k+\frac{\mu\tilde{D}_{1K}^{eff}\tilde{D}_{2K}^{eff}}{RTc_t(\tilde{D}_{12}^{eff}+y_2\tilde{D}_{1K}^{eff}+y_1\tilde{D}_{2K}^{eff})} \quad (15d)$$

$$N_l^{convection}=-\overline{c_2}\frac{\overline{k_2}}{\mu}\nabla p \quad (15e)$$

$$N_l^{\delta}=\overline{N_2^{\delta}}=\left(\frac{\tilde{D}_{1K}^{eff}\tilde{D}_{2K}^{eff}y_2}{\tilde{D}_{12}^{eff}+y_2\tilde{D}_{1K}^{eff}+y_1\tilde{D}_{2K}^{eff}}\right)\Delta = \frac{\tilde{D}_{2K}^{eff}y_2}{\tilde{D}_{12}^{eff}+y_2\tilde{D}_{1K}^{eff}+y_1\tilde{D}_{2K}^{eff}}\sum_{i\neq l}N_i\left(\frac{\tilde{D}_{21}^{eff}D_{iK}^{eff}-D_{li}^{eff}\tilde{D}_{1K}^{eff}}{D_{li}^{eff}D_{iK}^{eff}}\right). \quad (15f)$$

The contribution of N_l^{δ} to N_l couples N_l with other $N_{i\neq l}$, but this contribution is likely to be small due to the cancellation factor $(\tilde{D}_{21}^{eff}D_{iK}^{eff}-D_{li}^{eff}\tilde{D}_{1K}^{eff})$ shown in Eq. (15f) that is exactly equal to zero for binary mixtures. Assuming that N_l^{δ} is negligible, the molar flux of any given species l can be simply calculated as:

$$N_l=N_l^{diffusion}+N_l^{convection}=-\overline{D_2}\nabla\overline{c_2}-\overline{c_2}\frac{\overline{k_2}}{\mu}\nabla p \quad (16)$$

That is, as in FM, the molar flux of any species may be calculated independently in the simplified DGM (Eq. (16)) as long as the gas properties and distribution are given. Eq. (16) is called the DGMFM because it is simple, as an FM is, and has a computational accuracy that is similar to that of the DGM if N_l^{δ} is indeed negligible. In the following section, the accuracy of Eq. (16) for predicting multicomponent gas transport in an SOFC anode will be systematically tested for a wide range of scenarios.

3. Numerical model for testing the DGMFM

3.1. Model description

In an operating SOFC, a fuel mixture is continuously supplied to an SOFC cell from the fuel channel inlet, as shown in Fig. 1. Gas molecules in the fuel stream diffuse from the fuel channel to reaction sites in the porous anode, where they are oxidized and converted into products. The products are then transported back to the fuel channel and removed from the fuel channel outlet. Because the fuel composition is different at different locations in the channel-anode interface, a 3D model is generally required to fully describe the mass transport in the anode. However, a 1D model (in the z-direction) is suitable for testing the accuracy of the DGMFM if different fuel compositions are included in the test cases.

The molar mass conservation equation of species i in the 1D model is given according to the steady state condition by:

$$\frac{\partial N_i}{\partial z}=R_i \quad (17)$$

where R_i is the molar rate of production (+) or consumption (−) of species i due to chemical/electrochemical reactions. N_i can be calculated either by the DGMFM (Eq. (16)) or by the DGM (Eq. (1)).

In the following test of the DGMFM, the fuel is a mixture of methane (CH_4), steam (H_2O), carbon monoxide (CO), hydrogen (H_2) and carbon dioxide (CO_2). Methane steam reforming ($CH_4+H_2O\leftrightarrow CO+3H_2$) and the water gas-shift reaction ($CO+H_2O\leftrightarrow CO_2+H_2$) in the porous anode are explicitly considered. The rate of methane steam reforming ($mol\,m^{-3}\,s^{-1}$) is calculated as [3,8,39]:

$$R_r=S_A^{Ni}\left(0.0636T^2\ \exp\left(-\frac{27063}{T}\right)c_{CH_4}c_{H_2O}-3.7\times10^{-23}T^4\exp\left(-\frac{232.78}{T}\right)c_{CO}c_{H_2}^3\right) \quad (18)$$

where S_A^{Ni} is the volumetric active surface area of N_i particles ($m^2\,m^{-3}$). The shift reaction rate ($mol\,m^{-3}\,s^{-1}$) is determined as [3,8,39]:

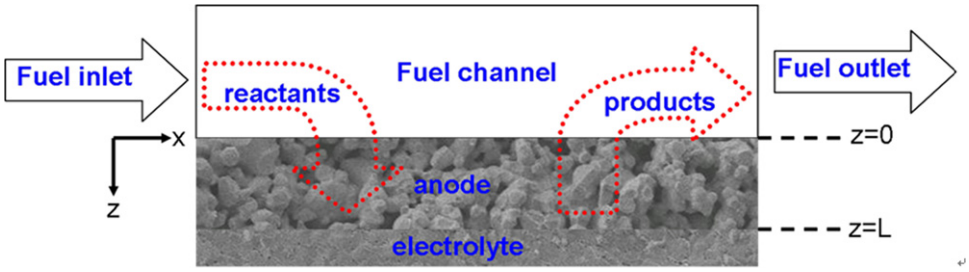

Fig. 1. A cross-section of an anode-supported SOFC.

$$R_S = \varepsilon\left(1.199T^2 \exp\left(-\frac{12509}{T}\right) c_{CO}c_{H_2O} - 67.7T^2 \exp\left(-\frac{16909}{T}\right) c_{CO_2}c_{H_2}\right) \quad (19)$$

In accordance with common observations, we assume here that the electrochemical conversion of CO is negligible compared with the rate of the water–gas shift reaction and that the electrochemical conversion of H_2 occurs at the anode–electrolyte interface. The molar flux of hydrogen at the anode–electrolyte interface ($z = L$ in Fig. 1) is calculated according to the Faraday law:

$$N_{H_2}\Big|_{z=L} = \frac{J_0}{2F} \quad (20)$$

where J_0 is the operating current density and F is Faraday's constant.

3.2. Numerical method and base model parameters

The finite element commercial software COMSOL MULTIPHYSICS® Version 3.5 [30] was employed for the solution of the model described above based on the DGMFM flux relations to obtain the species concentration distributions inside the porous anode. The numerical solutions based on the coupled DGM flux relations were obtained using the symbolic matrix inversion algorithm proposed by Zhu and Kee [13].

The basic model parameters and boundary conditions are summarized in Table 1. These parameters are representative of practical applications. They are used for all test cases unless explicitly stated otherwise.

Table 1
The base model parameters and boundary conditions.

Parameter	Value	Unit
Temperature (T)	1073.15	K
Anode permeability (k)	2.0E−14	m^{-2}
Viscosity coefficient (μ)	2.8E−5	Pa s
Average pore radius (r_g)	2.5E−7	m
Thickness (L)	7.5E−4	m
Porosity (ε)	0.3	
Tortuosity factor (τ)	3	
Specific active surface area of Ni (S_A^{Ni})	2.0E5	m^{-1}
Diffusion volume of H2 (ν_{H_2})	6.12E−6	$m^3\ mol^{-1}$
Diffusion volume of H_2O (ν_{H_2O})	1.31E−5	$m^3\ mol^{-1}$
Diffusion volume of CH_4 (ν_{CH_4})	2.514E−5	$m^3\ mol^{-1}$
Diffusion volume of CO (ν_{CO})	1.8E−5	$m^3\ mol^{-1}$
Diffusion volume of CO_2 (ν_{CO_2})	2.67E−5	$m^3\ mol^{-1}$
Mole fraction of H_2 at the channel/anode interface	0.263	
Mole fraction of H_2O at the channel/anode interface	0.2	
Mole fraction of CH_4 at the channel/anode interface	0.171	
Mole fraction of CO at the channel/anode interface	0.36	
Mole fraction of CO_2 at the channel/anode interface	0.006	
Operating current density	1.0E4	$A\ m^{-2}$
Total gas pressure at the channel/anode interface	1	atm

The validity and the prediction capability of the proposed DGMFM should be tested for a variety of possible parameters that may affect gas transport in a porous medium. These parameters may be broadly classified into two categories. One category includes the structural parameters of the porous medium such as the pore size, porosity, tortuosity and the thickness of the SOFC anode. The other category includes the operating parameters of the SOFC such as the current density, temperature and fuel composition. The tests are therefore divided into three scenarios: the accuracy of the DGMFM for the base model, the accuracy of the DGMFM for different anode structures and the accuracy of the DGMFM for different operating conditions.

4. Results and discussion

4.1. The accuracy of the DGMFM for the base model

Fig. 2 shows the distributions of the mole fractions of the species of all fuel components in the anode as predicted by the DGM and the DGMFM. Clearly, the DGMFM results agree very well with the DGM results, indicating that the assumption that the contribution of N_l^{δ} (Eq. (15)) to the species flux can be neglected is a highly accurate approximation for the base test case. Because the DGMFM and the DGM results for the species distributions are effectively indistinguishable, the computed quantities such as the concentration polarization, the chemical reaction rates and the associated heat generation are also effectively indistinguishable. In other words, the proposed DGMFM reproduces the physics of the DGM very well, and the DGMFM is a highly accurate replacement for the DGM for the representative base model.

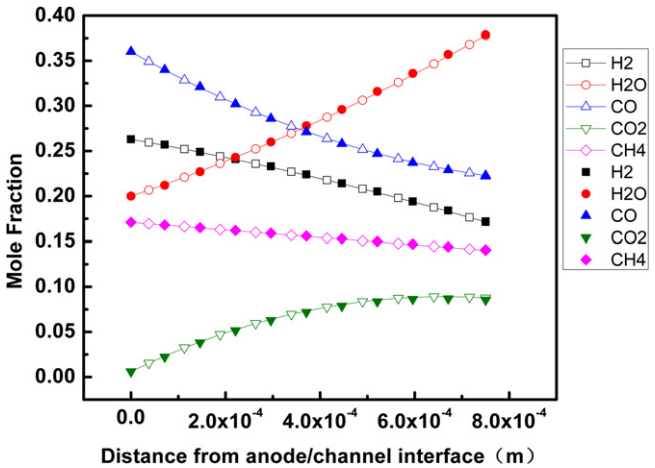

Fig. 2. Distributions of fuel species in an anode as predicted by the DGMFM (lines + open symbols) and the DGM (solid symbols) for the base model.

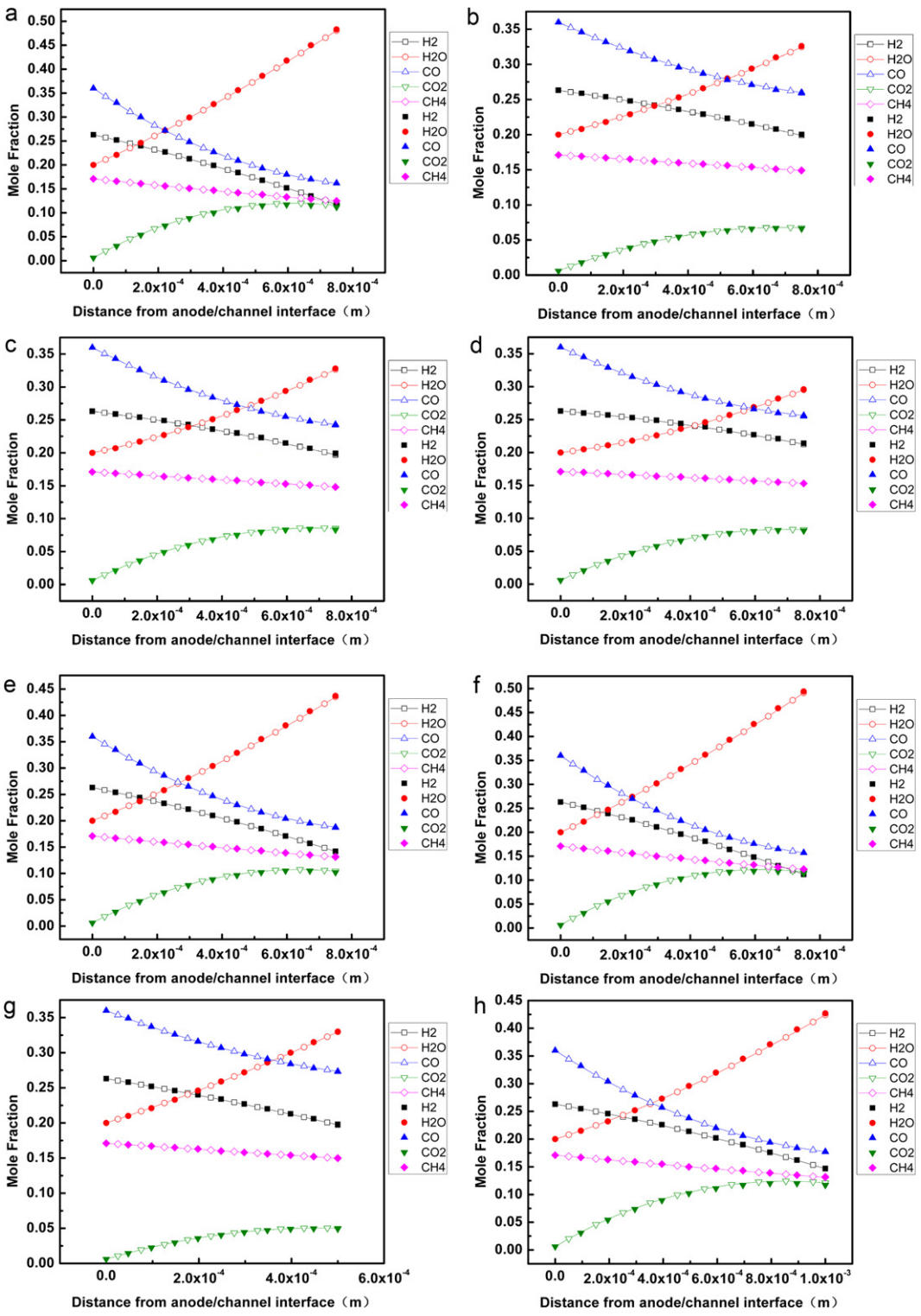

Fig. 3. Distributions of fuel species in an anode as predicted by the DGMFM (lines + open symbols) and the DGM (solid symbols): (a) r_g = 1.25E−7 m, (b) r_g = 5E−7 m, (c) ε = 0.4, (d) ε = 0.5, (e) τ = 4, (f) τ = 5, (g) L = 500 μm, and (h) L = 1000 μm.

4.2. The accuracy of the DGMFM for varying porous medium structures

Because the Knudsen diffusion coefficient is proportional to the pore radius (Eq. (3)), the pore radius is a key parameter that controls gas transport in the SOFC porous electrode. A mass transport model suitable for large pore sizes may not be appropriate for small pore sizes [14]. The pore sizes may vary for different designs and may be affected by the manufacturing processes used for the electrodes [40,41]. A sensitivity test of the accuracy of the DGMFM as a function of the pore radius is therefore important. Fig. 3a and b compares the predictions of the DGM and the DGMFM for r_g = 1.25E−7 m and r_g = 5E−7 m. It is apparent that the species distributions predicted by the DGMFM and the DGM agree very well with each other.

Both the Knudsen diffusion coefficient (Eq. (3)) and the effective binary diffusion coefficient (Eq. (2)) are proportional to the

porosity. Increasing the porosity leads to a reduced mass transport resistance and, consequently, reduced species concentration gradients. Moreover, the shift reaction rate increases with increasing porosity (Eq. (19)) because the shift reaction occurs wherever the gas is present. Therefore, changing the porosity may affect the species distributions via multiple mechanisms, providing a way to test the accuracy of the DGMFM for explicitly coupled effects. Fig. 3c and d shows the results of the DGM and the DGMFM for different porosities. Again, the DGMFM and the DGM results are effectively the same.

The tortuosity factor of an SOFC anode is typically between 2 and 6 [8,42,43]. Increasing the tortuosity factor of an anode increases the mass transport resistance via the reduced effective binary diffusion coefficient (Eq. (2)) and the Knudsen diffusion coefficient (Eq. (3)) due to the increased effective diffusion path length, resulting in increased mole fraction gradients for the individual species. Therefore, the species distributions are sensitive to the tortuosity factor. Fig. 3e and f depicts the mole fraction distributions of the gas species in an anode as predicted by the DGM and the DGMFM for different tortuosity factors. The results show that the DGMFM is capable of accurately reproducing the DGM results for different tortuosity factors.

A thicker anode layer corresponds to a higher mass transport resistance. The hydrogen mole concentration and the total gas pressure at the anode–electrolyte boundary must be properly balanced to produce the required H_2 flux imposed by the given operating current density (Eq. (20)). Consequently, the gas species distribution is sensitive to the anode thickness. Fig. 3g and h shows comparisons of the mole fraction distributions of the species in the anode as predicted by the DGMFM and the DGM for different anode thicknesses. Evidently, the DGMFM is highly accurate in reproducing the DGM results for different anode thicknesses.

4.3. The accuracy of the DGMFM for varying operating parameters

An SOFC may operate under different working conditions such as the operating temperature (T), output current density (J_0) and fuel composition. The validity of the DGMFM for the different working conditions that may affect mass transport in the porous anode requires verification. Because the chemical and electrochemical reaction rates and both the binary and Knudsen diffusion coefficients are temperature dependent, mass transport in the anode may be substantially affected by the working temperature. Fig. 4a and b shows the mole fraction distributions of different gas species in the anode as predicted by the DGM and the DGMFM for the constant current density of 1.0E4 A m^{-2} and the working temperatures of T = 873.15 K and T = 973.15 K. A comparison of Figs. 2, 4a and b show that the mole fractions of H_2 and CO_2 in the anode are higher at the higher temperature due to the higher rates of methane steam reforming and the water shift reaction. However, the good agreement between the DGMFM and DGM results is not affected by the working temperature.

Because the hydrogen flux must be adjusted to meet the required output current density, the fuel species distributions are affected by the working current density. Fig. 4c–e compares the distributions of the mole fractions of the fuel species in the anode obtained with the DGM and the DGMFM for different operating current densities varying from 0.3 to 1.5 A cm^{-2}. Clearly, the DGMFM is highly accurate for all practical working current densities.

A working SOFC cell may be fed fuels with different compositions. Three different fuels reported in the literature are used to investigate the effect of the fuel composition on the accuracy of the DGMFM. The compositions of the three fuels are shown in Table 2. The predictions of the DGM and the DGMFM for the species mole fraction distributions in the anode for the three fuels are shown in Fig. 4f–h. The results show that the DGM and DGMFM results are effectively the same for all test cases. In other words, the DGMFM is highly accurate and is general applicable for fuels with different compositions.

Table 2
Different fuel compositions for testing the accuracy of the DGMFM.

Fuel compositions	Fuel_1 [44–46]	Fuel_2 [27]	Fuel_3 [2]
Mole fraction of H_2 at the channel/anode interface	0.263	0.13	0.353
Mole fraction of H_2O at the channel/anode interface	0.493	0.435	0.413
Mole fraction of CH_4 at the channel/anode interface	0.171	0.217	0.142
Mole fraction of CO at the channel/anode interface	0.029	0.085	0.013
Mole fraction of CO_2 at the channel/anode interface	0.044	0.133	0.079

4.4. Reasons for the high performance of the DGMFM

As shown above, the DGMFM is highly accurate in reproducing the DGM results for many possible variations of the model parameters. Clearly, neglecting the contribution of N_l^δ to the species flux N_l (Eq. (14)) in any of the test cases leads to only a very small absolute error in the species distribution. In other words, the contribution of N_l^δ to N_l is very small overall. Taking into account that N_l may change signs and be zero or very close to zero in some regions, for convenience, we use the absolute flux averages to measure the magnitude of N_l^δ relative to N_l:

$$\overline{N_l^{diffusion}} = \frac{1}{L}\int_0^L \left|N_l^{diffusion}\right| dz \tag{21a}$$

$$\overline{N_l^{convection}} = \frac{1}{L}\int_0^L \left|N_l^{convection}\right| dz \tag{21b}$$

$$\overline{N_l^{\delta}} = \frac{1}{L}\int_0^L \left|N_l^{\delta}\right| dz \tag{21c}$$

$$\overline{N_l} = \overline{N_l^{diffusion}} + \overline{N_l^{convection}} + \overline{N_l^{\delta}} \tag{21d}$$

The relative significances of the flux components to the overall species flux may be measured as:

$$\gamma_l^d = \frac{\overline{N_l^{diffusion}}}{\overline{N_l}} \tag{22a}$$

$$\gamma_l^c = \frac{\overline{N_l^{convection}}}{\overline{N_l}} \tag{22b}$$

$$\gamma_l^\delta = \frac{\overline{N_l^{\delta}}}{\overline{N_l}} \tag{22c}$$

Table 3 shows the values of $\overline{N_l}$, γ_l^d, γ_l^c and γ_l^δ for the base test case. As can be seen in Table 3, the values of γ_l^δ are very small, and the maximum γ_l^δ is only 1.4%. Therefore, at least for the base case,

Table 3
Species fluxes and flux components for the base model.

Species	$\overline{N_l}$ (mol (m^{-2} s^{-1}))	γ_l^d (%)	γ_l^c (%)	γ_l^δ (%)
H_2	0.052	87.9	11.7	0.4
H_2O	0.040	80.4	19.5	0.1
CH_4	0.010	51.4	47.2	1.4
CO	0.026	70.1	28.7	1.2
CO_2	0.012	84.2	15.7	0.1

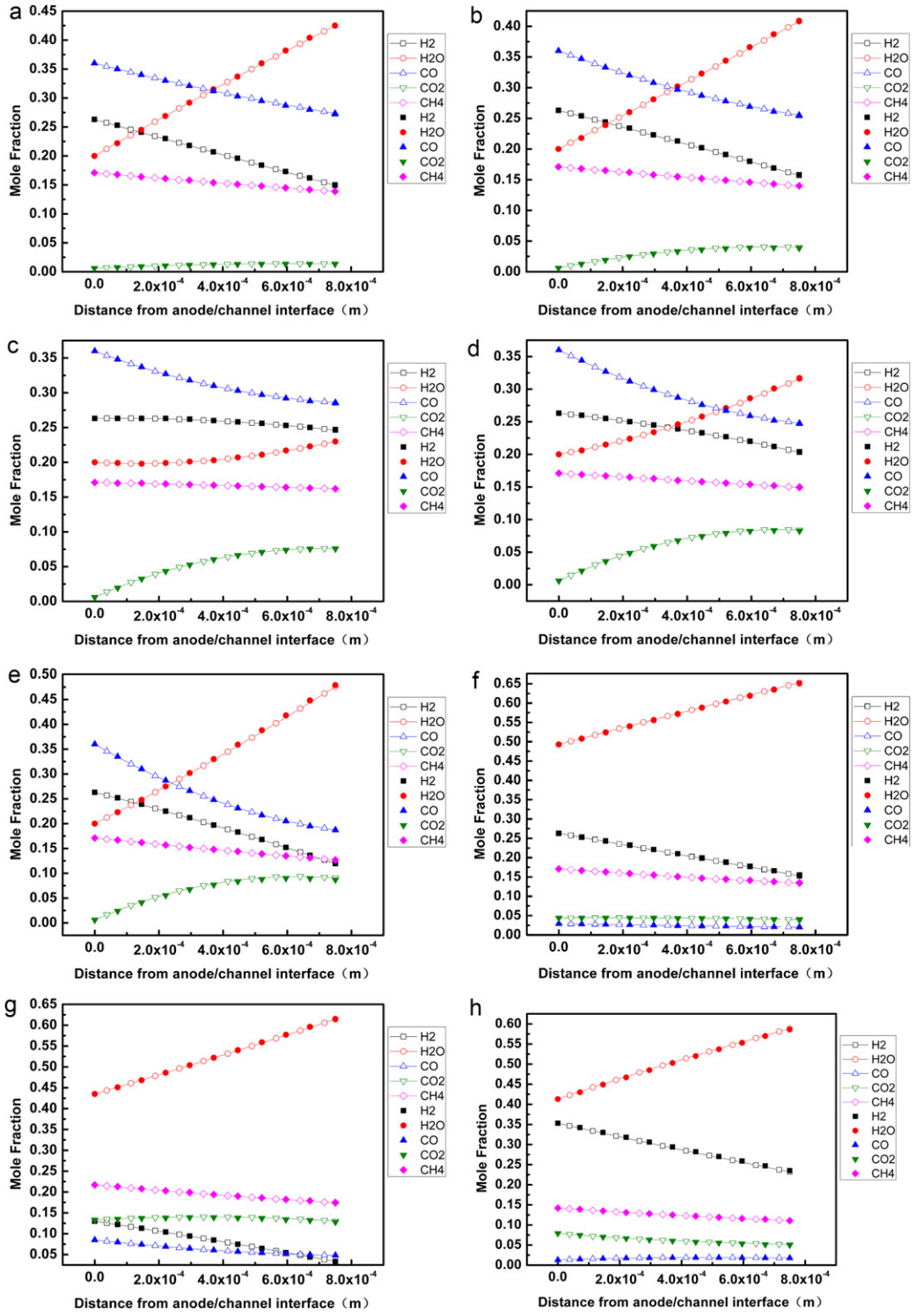

Fig. 4. Distributions of fuel species in an anode as predicted by the DGMFM (lines + open symbols) and the DGM (solid symbols): (a) $T = 873.15$ K, (b) $T = 973.15$ K, (c) $J_0 = 0.3\ \mathrm{A\,cm^{-2}}$, (d) $J_0 = 0.7\ \mathrm{A\,cm^{-2}}$, (e) $J_0 = 1.5\ \mathrm{A\,cm^{-2}}$, (f) Fuel_1 (g) Fuel_2, and (h) Fuel_3.

the assumption that the contribution of N_l^δ to the species flux can be neglected is a very good approximation. To show that N_l^δ can generally be neglected, Fig. 5 shows the results of γ_l^d, γ_l^c and γ_l^δ for all of the above test cases. As shown in Fig. 5, γ_l^δ is always small and negligible (the maximum γ_l^δ for all of the test cases is merely 2%). Thus, the DGMFM is an excellent representation of the DGM in all cases.

As an aside, it is worth pointing out that, except for $l = H_2$, the relative magnitudes of the diffusion and convection fluxes, γ_l^d and γ_l^c, are comparable in numerous cases, as shown in Fig. 5. In particular, the convection flux of CH_4 is comparable to the diffusion flux of CH_4 in all of the test cases. This is in sharp contrast to the common belief that the diffusion flow in a porous medium is more important than the convective flow [16,18]. The direct use of FM is certain to produce inaccurate results.

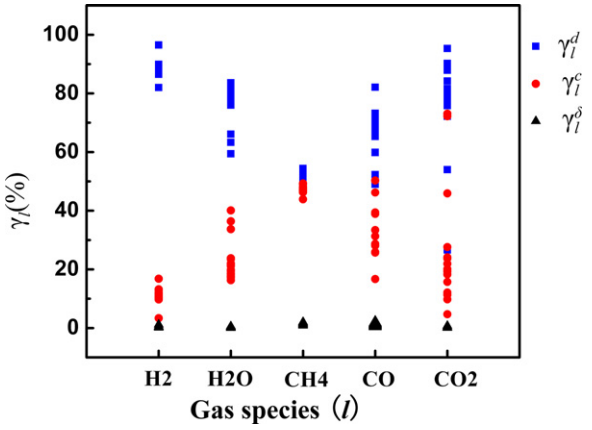

Fig. 5. The relative magnitudes of the species flux components, γ_l^d (rectangles), γ_l^c (circles) and γ_l^δ (triangles), for all of the tested cases.

5. Conclusions

An approximate DGM in the form of Fick's model, the DGMFM, is developed. The model gives explicit analytical expressions for the fluxes of species that are decoupled from one another, and the model may easily be combined with the mass conservation equation for solving multicomponent mass transport in porous media. Numerical tests on the new method are performed by systematically varying the structural and operating parameters that may affect mass transport in the SOFC anode. All tests consistently show that the new model is highly accurate in reproducing the results of the DGM. Therefore, the DGMFM can replace the DGM for analyzing multicomponent mass transport in porous media.

Acknowledgements

The financial support of the State Key Development Program for Basic Research of China (Grant No. 2012CB215405), the Key Program of the Chinese Academy of Sciences (KJCX1.YW.07) and the National Natural Science Foundation of China (10574114) are gratefully acknowledged. The authors thank Prof. Haiqian Wang for providing the SEM image of a porous SOFC anode shown in Fig. 1.

References

[1] C.O. Colpan, I. Dincer, F. Hamdullahpur, Int. J. Energy Res. 32 (2008) 336–355.
[2] R.J. Kee, H.Y. Zhu, A.M. Sukeshini, G.S. Jackson, Combust. Sci. Technol. 180 (2008) 1207–1244.
[3] J. Klein, Y. Bultel, S. Georges, M. Pons, Chem. Eng. Sci. 62 (2007) 1636–1649.
[4] T. Yamaguchi, S. Shimizu, T. Suzuki, Y. Fujishiro, M. Awano, Electrochem. Commun. 10 (2008) 1381–1383.
[5] Y. Jiang, A.V. Virkar, J. Electrochem. Soc. 150 (2003) A942.
[6] S. Liu, C. Song, Z. Lin, J. Power Sources 183 (2008) 214–225.
[7] S.H. Chan, K.A. Khor, Z.T. Xia, J. Power Sources 93 (2001) 130–140.
[8] W. Lehnert, J. Meusinger, F. Thom, J. Power Sources 87 (2000) 57–63.
[9] J. Phattaranawik, R. Jiraratananon, A.G. Fane, J. Membr. Sci. 215 (2003) 75–85.
[10] R. Krishna, J.A. Wesselingh, Chem. Eng. Sci. 52 (1997) 861–911.
[11] A.S. Joshi, A.A. Peracchio, K.N. Grew, W.K.S. Chiu, J. Phys. D: Appl. Phys. 40 (2007) 7593–7600.
[12] M. Cannarozzo, A.D. Borghi, P. Costamagna, J. Appl. Electrochem. 38 (2008) 1011–1018.
[13] H. Zhu, R.J. Kee, V.M. Janardhanan, O. Deutschmann, D.G. Goodwin, J. Electrochem. Soc. 152 (2005) A2427–A2440.
[14] R. Suwanwarangkul, E. Croiset, M.W. Fowler, P.L. Douglas, E. Entchev, M.A. Douglas, J. Power Sources 122 (2003) 9–18.
[15] B. Kenney, M. Valdmanis, C. Baker, J.G. Pharoah, K. Karan, J. Power Sources 189 (2009) 1051–1059.
[16] J.W. Veldsink, G.F. Versteeg, W.P.M. Van Swaaij, R.M.J. Van Damme, Chem. Eng. J. Biochem. Eng. J. 57 (1995) 115–125.
[17] S.W. Webb, K. Pruess, Transport in Porous Media 51 (2003) 327–341.
[18] Y. Vural, L. Ma, D.B. Ingham, M. Pourkashanian, J. Power Sources 195 (2010) 4893–4904.
[19] S. Kakac, A. Pramuanjaroenkij, X.Y. Zhou, Int. J. Hydrogen Energy 32 (2007) 761–786.
[20] J.B. Duncan, H. Toor, AIChE J. 8 (1962) 38–41.
[21] D.C. Thorstenson, D.W. Pollock, Water Resour. Res. 25 (1989) 477–507.
[22] A.L. Baehr, C.J. Bruell, Water Resour. Res. 26 (1990) 1155–1163.
[23] R.B. Bird, W.E. Stewart, E.N. Lightfoot (Eds.), Transport Phenomenon, 2nd ed., John Wiley & Sons, New York, 2002.
[24] E.A. Mason, A.P. Malinauskas, Transport in Porous Media: The Dusty Gas Model, Elsevier, New York, 1983.
[25] F.N. Cayan, S.R. Pakalapati, F. Elizalde-Blancas, I. Celik, J. Power Sources 192 (2009) 467–474.
[26] T.X. Ho, P. Kosinski, A.C. Hoffmann, A. Vik, Int. J. Hydrogen Energy 34 (2009) 3488–3499.
[27] K. Nikooyeh, A.A. Jeje, J.M. Hill, J. Power Sources 171 (2007) 601–609.
[28] Fluent 6. 3 User's Guide, Fluent Inc., 2006.
[29] ANSYS CFX 13.0 help document, Ansys Inc., 2010.
[30] COMSOL MULTIPHSICS® Version 3.5 User's Guide, COMSOL. AB, 2007.
[31] K.W. Lawson, D.R. Lloyd, J. Membr. Sci. 120 (1996) 123–133.
[32] K.R. Kaza, R. Jackson, Chem. Eng. Sci. 35 (1980) 1179–1187.
[33] S.W. Webb, J.M. Phelan, J. Contam. Hydrol. 27 (1997) 285–308.
[34] S. Molins, K. Mayer, R. Amos, B. Bekins, J. Contam. Hydrol. 112 (2010) 15–29.
[35] R. Evans, G. Watson, J. Truitt, J. Appl. Phys. 33 (1962) 2682–2688.
[36] S. Liu, W. Kong, Z. Lin, J. Power Sources 194 (2009) 854–863.
[37] E.N. Fuller, P.D. Schettler, J.C. Giddings, Ind. Eng. Chem. 58 (1966) 18–27.
[38] B. Todd, J.B. Young, J. Power Sources 110 (2002) 186–200.
[39] K. Hou, R. Hughes, Chem. Eng. J. 82 (2001) 311–328.
[40] D.H. Jeon, J.H. Nam, C.J. Kim, J. Electrochem. Soc. 153 (2006) A406–A417.
[41] D. Chen, Z. Lin, H. Zhu, R.J. Kee, J. Power Sources 191 (2009) 240–252.
[42] R. Williford, L. Chick, Surf. Sci. 547 (2003) 421–437.
[43] R.E. Williford, L.A. Chick, G.D. Maupin, S.P. Simner, J.W. Stevenson, J. Electrochem. Soc. 150 (2003) A1067.
[44] M. Ni, D.Y.C. Leung, M.K.H. Leung, J. Power Sources 183 (2008) 133–142.
[45] Y.W. Kang, J. Li, G.Y. Cao, H.Y. Tu, J. Yang, Chin. J. Chem. Eng. 17 (2009) 304–317.
[46] Q. Wang, L. Li, C. Wang, J. Power Sources 186 (2009) 399–407.